university of groningen

University Medical Center Groningen

University of Groningen

Stress analysis and microstructure of PVD monolayer TiN and multilayer TiN/(Ti,Al)N coatings

Carvalho, NJM; Zoestbergen, E; Kooi, BJ; De Hosson, JTM

Published in:
Thin Solid Films

DOI:
10.1016/S0040-6090(03)00067-1

IMPORTANT NOTE: You are advised to consult the publisher's version (publisher's PDF) if you wish to cite from it. Please check the document version below.

Document Version
Publisher's PDF, also known as Version of record

Publication date:
2003

Link to publication in University of Groningen/UMCG research database

Citation for published version (APA):
Carvalho, NJM., Zoestbergen, E., Kooi, BJ., & De Hosson, JTM. (2003). Stress analysis and microstructure of PVD monolayer TiN and multilayer TiN/(Ti,Al)N coatings. *Thin Solid Films*, *429*(1-2), 179-189. https://doi.org/10.1016/S0040-6090(03)00067-1

Copyright
Other than for strictly personal use, it is not permitted to download or to forward/distribute the text or part of it without the consent of the author(s) and/or copyright holder(s), unless the work is under an open content license (like Creative Commons).

The publication may also be distributed here under the terms of Article 25fa of the Dutch Copyright Act, indicated by the “Taverne” license. More information can be found on the University of Groningen website: https://www.rug.nl/library/open-access/self-archiving-pure/taverne-amendment.

Take-down policy
If you believe that this document breaches copyright please contact us providing details, and we will remove access to the work immediately and investigate your claim.

Downloaded from the University of Groningen/UMCG research database (Pure): http://www.rug.nl/research/portal. For technical reasons the number of authors shown on this cover page is limited to 10 maximum.

Download date: 04-05-2023

Available online at www.sciencedirect.com
SCIENCE DIRECT®
Thin Solid Films 429 (2003) 179–189
thin solid films
www.elsevier.com/locate/tsf

Stress analysis and microstructure of PVD monolayer TiN and multilayer TiN/(Ti,Al)N coatings

N.J.M. Carvalho, E. Zoestbergen[1], B.J. Kooi, J.Th.M. De Hosson*

Department of Applied Physics, Materials Science Centre and Netherlands Institute for Metals Research, University of Groningen, Nijenborgh 4, 9747 AG Groningen, The Netherlands

Received 9 November 2002; received in revised form 20 January 2003; accepted 24 January 2003

Abstract

Two PVD titanium nitride based coatings; monolayer TiN and multilayer resulting from the stacking of TiN and (Ti,Al)N layers were evaluated with respect to their stress state and microstructure. The TiN was deposited by triode evaporation ion plating, whereas the TiN/(Ti,Al)N was deposited using a reactive hybrid deposition process consisting of a combination of electron beam evaporation of Ti and DC magnetron sputtering of a Ti–Al alloy. The structural and mechanical state characterisations of the as-deposited coatings on steel substrates were performed using X-ray diffraction methods. The Bragg–Brentano geometry was used to study the texture and the $\sin^2\psi$ method was applied to obtain the stress-free lattice parameter, the Poisson's ratio and the residual stresses. The monolayer exhibited a preferred orientation with (1 1 1) parallel to the surface. However, the TiN and (Ti,Al)N layers from the multilayer revealed a slightly (3 1 1) preferred orientation. All coatings were in a state of compressive stress ranging from 10.1 to 2.7 GPa, depending logically on the substrate material, layer thickness and deposition processes. The microstructure and composition of the coatings were investigated using a combination of scanning electron microscopy, plan-view and cross-sectional transmission electron microscopy, energy-dispersive spectroscopy and electron energy-loss spectroscopy. The TiN exhibited a fibrous microstructure where only a few columns extended through the whole coating thickness. The TiN/(Ti,Al)N multilayer revealed a more pronounced columnar microstructure with the columns extending throughout the film thickness. Micrometer-sized macroparticles were present in the multilayer at various distances from the substrate, but never at the substrate surface. The results showed that they were incorporated in the growing film in the solid state and consisted of a core structure with equiaxed grains having the α-Ti phase and an outer layer of TiN. Evidence was found of nitrogen diffusion, presumably from both the working gas into the solidifying Ti droplet during migration to the film and through the TiN outer layer.
© 2003 Elsevier Science B.V. All rights reserved.

Keywords: PVD coatings; TiN and TiN (Ti, Al)N; Residual stress; Macroparticles

1. Introduction

It is indisputable that TiN deposited as a monolayer holds a dominant position in the field of hard coatings to improve the wear resistance of high speed steel cutting tool, punches and metal forming components [1,2]. However, a drawback of such coatings is their limited oxidation resistance at temperatures above 600 °C where a TiO_2 layer is formed. Due to the large difference in molar volumes between the TiO_2 and TiN, compressive stresses are developed in the oxide layer resulting in spallation and exposure of unoxidised nitride to further oxidation [3,4].

In the recent years, considerable efforts have been devoted to the development of both multi-component constituents and multilayered structures so as to further improve the wear resistance of coated components. The improvement is expected to be accomplished by alternately depositing two (or more) chemically and/or mechanically different materials in such a way that the stress concentration and the conditions for crack propagation can be controlled. Therefore the multilayer struc-

*Corresponding author. Tel.: +31-50-3634898; fax: +31-50-3634881.
E-mail address: hossonj@phys.rug.nl (J.Th.M. De Hosson).
[1] Present address: Fraunhofer Institute Materials and Beam Technology, Winterbergstraße 28, 01277 Dresden, Germany.

0040-6090/03/$ - see front matter © 2003 Elsevier Science B.V. All rights reserved.
doi:10.1016/S0040-6090(03)00067-1

ture may act as a crack inhibitor, thereby increasing the coating fracture resistance [5,6]. Further, the properties of the surface can also be improved by combining layers that individually have different effects on the overall performance. The multilayer coating investigated in this paper consisted of a superlattice structure of TiN and (Ti,Al)N layers and was deposited to take advantage of single layer materials properties. Hence, a interfacial layer of TiN was used to improve the adhesion between the substrate and the coating, and a (Ti,Al)N top layer to increase the oxidation resistance at elevated temperatures.

The coatings were provided, and are commercialised, by Balzers AG, Liechtenstein. They were deposited using the growth parameters close to, or identical with, those used for production (as of 2000). It should be pointed out at the outset that the aim of this paper is to provide a better understanding of the intrinsic relationships between the chemical composition, the stress state and the microstructure of monolayer TiN and multilayered TiN/(Ti,Al)N coatings, grown by commercially available processes. Further, questions concerning detailed deposition parameters and reproducibility should be addressed to the manufacturer.

Transmission electron microscopy (TEM) was used as the primary technique. By combining direct imaging and electron diffraction it was possible to obtain detailed information about phase composition, grain size and shape, and degree of preferred orientation. Nevertheless complementary techniques such as analytical TEM, scanning electron microscopy (SEM), and X-ray diffraction (XRD) were also used to provide complimentary information concerning the microchemistry, morphology, residual stress state, and phase composition of the systems.

2. Experimental details

Two coatings were investigated, a monolayer TiN, and a multilayer coating consisting of alternating nanometer thick layers of TiN and (Ti,Al)N, designated by TiN/(Ti,Al)N. All coatings were deposited on both cold work tool steel (AISI D2) and stainless steel (AISI 304) substrates. The substrates materials were polished to mirror finish surfaces with R_a values of approximately 0.05 μm. The substrate hardness, elastic modulus, Poisson's ratios, and thermal expansion coefficients are given in Table 1.

Prior to insertion into the vacuum chamber, the substrates were ultrasonically cleaned in trichlorethylene, acetone, alcohol, and then dried with N_2 gas. The TiN coating was deposited in a Balzers BAI 640R coating unit fitted with an electron beam evaporation source (e-gun). The deposition process was based on the standard Balzers TiN process utilizing triode ion plating with high plasma density. The deposition

Table 1
Characteristics of the substrates used

Material	Hardness (GPa)	E-modulus (GPa)	Poisson's ratio	Expansion coefficient (10^{-6} K^{-1})
AISI 304	1.6	193	0.29	17.8–18.4
AISI D2	6.8	210	0.29	11.9–12.9

sequence consisted of pumping down the chamber, substrate heating and sputter-cleaning, and coating deposition. The vacuum chamber was evacuated to a base pressure less than 10^{-4} Pa. The substrates were electron heated to a temperature of 450 °C for 45 min and then sputter etched (Ar^+) with a negative substrate bias of 200 V for a further 15 min. The coating was deposited at 450 °C using a negative substrate bias of 110 V and the e-gun emission current was regulated in order to maintain a constant N_2 partial pressure of approximately 0.05 Pa.

The multilayer was deposited in a BAI 830PM coating unit with a hybrid process described in detail elsewhere [7]. In essence, it combines reactive ion plating deposition of TiN by high current density plasma beam evaporation and reactive magnetron sputtering for deposition of (Ti,Al)N from a titanium–aluminium alloy target. The deposition process consisted of exhausting the vacuum chamber to a pressure less than 5×10^{-4} Pa, then heating the substrates to a temperature of approximately 450 °C to outgas the surfaces. Thereafter the substrates were sputter etched (Ar^+) with a negative substrate bias of 1000 V. The coating deposition occurred at 450 °C with a constant partial pressure of N_2. A total thickness of 5.0 μm was aimed at for both coatings.

The coatings structure was determined by XRD measurements with the standard Bragg–Brentano geometry using a Philips PW710 based diffractometer with Cu Kα radiation and generator settings of 40 kV and 30 mA. The texture and stress state in the coatings were examined using a Philips X'Prt PW3040 diffractometer with a high resolution ψ goniometer and Cu Kα radiation. The stresses were calculated from the well-known $\sin^2\psi$ method. Analytical TEM was carried out using a JEOL 2010 FEG, operating at 200 kV, equipped with an EDAX energy dispersive analyser and a post-column Gatan imaging filter. Energy dispersive X-ray spectroscopy (EDS) analysis was performed by line profile in cross-sectional TEM (XTEM) specimens using a normal probe with FWHM of 0.5 nm. Electron energy filtered images were recorded using the so-called three-window technique, which consists of acquiring a series of two images at energy-losses preceding the ionisation edge and one image at an energy-loss behind the ionisation edge. The two pre-edge images were used for background extrapolation and subtraction from the post-edge

image. This procedure resulted in an elemental map with pixel values proportional to the actual concentration. The microstructure of the as-deposited coatings was studied by plan-view and cross-sectional TEM using a JEOL 4000 EX/II, operating at 400 kV. Specimen preparation for plan-view TEM consisted of cutting a disc out of the region of interest with 3 mm diameter using the Nd-YAG laser, followed by grinding and polishing from the substrate side to a thickness of 50 μm. The disc was further Ar^+ ion milled to electron transparency by etching the sample from the substrate side. The final etching was performed briefly from both sides with a reduced tilt angle. This was done in order to reduce ion induced artefacts and to remove any amorphous redeposited surface layer. The XTEM specimens were prepared by gluing two samples film-to-film in a 700 μm wide slot of a Ti disc. Subsequently the sample was mechanically ground and polished on both sides to a thickness of 50 μm. This was followed by ion beam milling using two guns in mirror-image positions on both sides of the sample. Subsequent thinning to electron transparency was accomplished by rocking the specimen ±30° perpendicular to the coating/substrate interface. Finally, the surface contaminants (due to redeposited material) were reduced by ion milling during a short time while continuously rotating the specimen. The incident beam angle started from 8° and was progressively reduced to 4° in the final stages of thinning.

3. Results and discussion

3.1. Crystal structure and residual stress state

Typical XRD diffraction patterns from monolayer TiN and multilayer TiN/(Ti,Al)N deposited onto stainless steel and of the bare substrate are shown in Fig. 1. The substrate displayed mainly reflections from the α-Fe and γ-Fe phases. TiN coatings were polycrystalline exhibiting diffraction peaks related to cubic δ-TiN phase. However, apparently the peaks had shifted towards lower diffracting angles with respect to their nominal ASTM positions. In fact the interplanar spacing d_{hkl} for the reflecting planes parallel to the surface determined from the XRD spectra showed, irrespectively of the substrate material, higher values than those from a randomly oriented strain-free standard sample, where d_{111} = 0.2449 nm. The value obtained for the (1 1 1) planes of the monolayer onto stainless steel and onto tool steel was 0.2464 and 0.2461 nm, respectively. This indicated that the coating was in a state of compressive stresses, which was in agreement with previous results on deposition of TiN [8]. The degree of preferred orientation of the coatings was determined by calculation of the texture coefficient, T_c [9]. The outcome revealed that the monolayer displayed a strong preferred (1 1 1) orientation parallel to the substrate surface. The presence of this texture was not surprising since the (1 1 1) plane in the TiN is the one of lowest strain energy due to anisotropy in the Young's modulus [10]. Therefore, the alignment normal to the growing direction minimised the total energy under strain energy dominated growth.

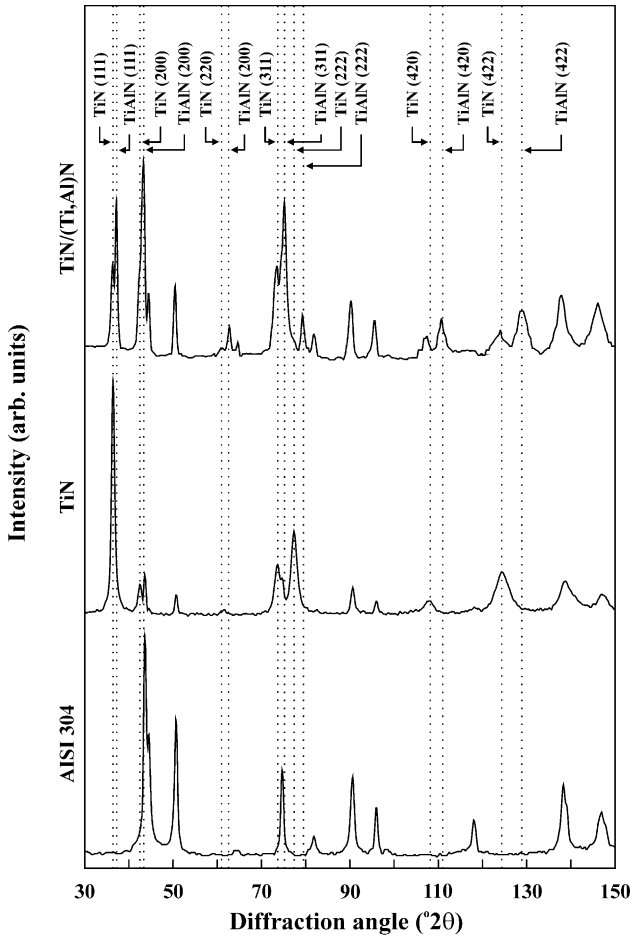

Fig. 1. XRD patterns of the multilayer TiN/(Ti,Al)N (top), monolayer TiN (middle), and bare substrate AISI 304 (bottom). The peaks that are not indexed correspond to the stainless steel substrate.

The TiN and (Ti,Al)N layers from the multilayer coating also exhibited the B1-NaCl crystal structure. The (Ti,Al)N peaks were shifted to lower interplanar spacing values with respect to the TiN peaks. The smaller lattice parameter was caused by the partial replacement of the titanium atoms in the TiN lattice by the aluminium, whose solubility limit is approximately 1.1 [11]. The small difference between the interplanar spacing of TiN and (Ti,Al)N layers made it very difficult to perform accurate textural analysis using the same method as for the monolayer. In this case intensity measurements were performed on the (4 2 2) plane demonstrating that both layers were slightly textured with a (3 1 1) preferred orientation. Stress measurements were carried out using the $\sin^2\psi$ method, where the

Table 2
Lattice parameter and Poisson's ratio of TiN and (Ti,Al)N

Parameter	TiN	(Ti,Al)N
d_0, nm	0.42430 ± 0.0001	0.4170 ± 0.0005
$\sin^2 \psi$	0.376 ± 0.003	0.301 ± 0.005
ν	0.232 ± 0.002	0.177 ± 0.003

lattice spacing of a particular $(h\,k\,l)$ plane as a function of its orientation was used as an internal strain gauge, and then the stresses were calculated by using the appropriate elastic constants [12]. By considering the layers isotropic and assuming a homogeneous biaxial state of the stress the lattice spacing $d^{hkl}_{\phi\psi}$ of the (4 2 2) plane had only to be measured for several directions inclined to the surface normal by an angle ψ. The angle ϕ was the rotational in the surface plane of the coating. The TiN and (Ti,Al)N layers from coatings on the stainless and tool steel substrates exhibited a linear relationship between the lattice spacing $d^{hkl}_{\phi\psi}$ and the $\sin^2 \psi$, with an intercept $I = d^{hkl}_{\phi\psi=0}$ and slope $M = \partial d^{hkl}_{\phi\psi} / \partial \sin^2\psi$. The unstressed lattice parameter d^{hkl}_0 was calculated as the intercept from the linear plot of the intercept I vs. the slope M. The slope $(\partial I / \partial M)$ provided the $\sin^2 \psi$ value for $d^{hkl}_{\phi\psi} = d^{hkl}_0$ from which the Poisson's ratio was calculated. The values obtained for the strain-free lattice spacing, the $\sin^2 \psi$, and the Poisson's ratio are given in Table 2 and were in good agreement with the values found in Ref. [13]. The residual stresses in (4 2 2) of the monolayer, and of the TiN and (Ti,Al)N layers from the multilayer, which were determined by the $\sin^2 \psi$ method with the measured X-ray elastic constants, are given in Table 3.

The residual stresses in the coatings deposited on tool steel were lower than on the ones deposited on stainless steel. This difference in magnitude was related to the residual stress being composed of an intrinsic component resulting from the growth process and an extrinsic component (thermal stress) that arose because of differences between the thermal expansion coefficients of the coating and the substrate. For coatings deposited on tool steel the extrinsic component had a minor effect because of the reduced difference in thermal expansion coefficient between the coating (9.4×10^{-6} K^{-1}) and the substrate (Table 1). As the thermal stresses in the TiN layers were assumed to be of the same magnitude as in the (Ti,Al)N layers, the higher compressive stresses observed in the TiN were due to an intrinsic origin. Oettel et al. [14] have demonstrated that with ion plating deposition—as was the case for the TiN layers in the multilayer—the so-called atomic or ion shoot peening effect is more pronounced than with sputtering processes (deposition of the (Ti,Al)N layers), thereby explaining the high stresses observed. Also the residual stress in the TiN layers of the multilayer was much higher than the stresses in the monolayer TiN. This difference may be in part due to the fact that the residual stresses in a PVD layer decrease as the layer thickness increases [15].

Table 3
Calculated residual stresses, assuming: $E = 450$ GPa; $\nu_{TiN} = 0.232$; $\nu_{TiAlN} = 0.177$

Plane	Coating–substrate	Residual stresses (GPa)
(4 2 2)	TiN–AISI 304	-5.6 ± 0.1
(4 2 2)	TiN layer[a]–AISI 304	-10.1 ± 0.3
(4 2 2)	(Ti,Al)N layer[b]–AISI 304	-4.2 ± 0.2
(4 2 2)	TiN–AISI D2	-4.2 ± 0.2
(4 2 2)	TiN layer[a]–AISI D2	-8.0 ± 0.4
(4 2 2)	(Ti,Al)N layer[b]–AISI D2	-2.7 ± 0.1

[a] TiN layer from the multilayer coating.
[b] (Ti,Al)N layer from the multilayer coating.

3.2. Microstructural analysis

The coatings thickness were close to 5.0 μm and no difference between the coatings deposited on stainless steel and tool steel substrate could be discerned, see Table 4. Fig. 2 shows representative SEM micrographs of the surface of the monolayer and the multilayer. The topography was typical for ion plating and sputtering deposition processes [16]. The former produced a smoother, shallow rippled surface, to a certain extent independent of the substrate roughness. The latter process resulted in a flatter surface with fine grains. However, it memorised the surface topography of the underlying substrate. As can be seen in Fig. 2b, grooves and ridges were still present. Nevertheless, the surface also displayed pronounced macroparticles and pinholes. The macroparticles were due to droplets that were incorporated during film growth, and the pinholes were the outcome of their debonding from the coating.

Fig. 3 shows a polished cross-sectional SEM micrograph of the multilayer obtained with a backscattered electron detector to emphasise the dissimilarity between TiN and (Ti,Al)N. TiN produces more backscattered electrons, and is therefore displayed as layers with brighter contrast. Although the multilayer had been defined as a stacking of TiN and (Ti,Al)N layers, the polished micrograph and TEM studies (see below) displayed their real structure, which consisted of a TiN

Table 4
Total coating thickness t_f, individual layer thickness $t_{(Ti,Al)N}$, superlattice thickness $t_{TiN-(Ti,Al)N}$, and surface roughness R_a

Coating–substrate	t_f (μm)	$t_{(Ti,Al)N}$ (nm)	$t_{TiN-(Ti,Al)N}$ (nm)	R_a (μm)
TiN–AISI 304	5.0 ± 0.1	–	–	0.06 ± 0.02
TiN–AISI D2	5.5 ± 0.1	–	–	0.09 ± 0.01
TiN/(Ti,Al)N–AISI 304	5.0 ± 0.1	122	11.8–9.2	0.28 ± 0.02
TiN/(Ti,Al)N–AISI D2	5.3 ± 0.1	122	11.8–9.2	0.23 ± 0.01

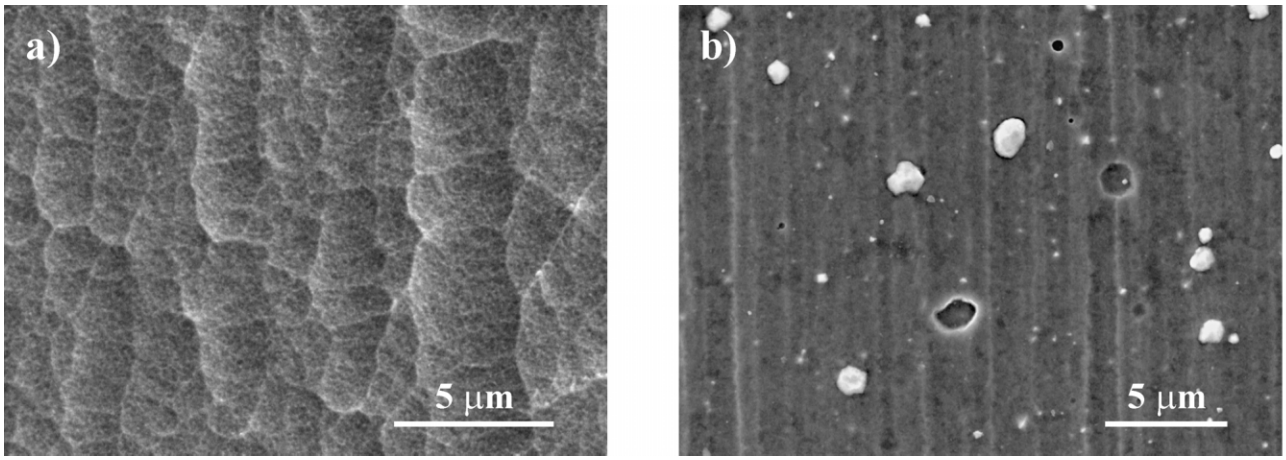

Fig. 2. Plan-view SEM micrographs displaying the surface morphology of (a) monolayer TiN and (b) multilayer TiN/(Ti,Al)N deposited onto tool steel substrate.

interfacial layer and a periodical structure with the following sequence: (Ti,Al)N/(TiN/(Ti,Al)N), i.e., the multilayer was composed of (Ti,Al)N layers and a superlattice of TiN and (Ti,Al)N, and finally of a thick (Ti,Al)N top layer given its higher oxidation resistance.

Fig. 4a and b are plan-view TEM images taken near the coating surface and Fig. 4c and d are the corresponding selected area electron diffraction (SAED) patterns. Both samples were polycrystalline with grain boundaries free of intergranular porosity and cracks. This feature sometimes made the grain boundaries difficult to observe. Therefore, one had to be careful in distinguishing large grains from clusters of extremely fine grains in close crystallographic orientation. Moreover, as one column might have consisted of several grains or subgrains, the grain size was often smaller than the column width. A high density of defects (dislocations) within the individual grains was also evident. Moiré fringes from the monolayer TiN were clearly visible. Because they resulted from destructive interference of diffracted waves due to overlapping grains it indicated that the TiN had a fibrous structure rather than columnar. The grain size distribution was homogeneous with an average size $\langle d \rangle$ of 50 nm. This small grain size was related to ion bombardment during film growth, which is known to create many radiation-induced defects in the growing film [17]. The defect density was sufficiently large to disrupt the columnar structure in such a way that new columns were nucleated periodically causing the suppression of large grains. The multilayer exhibited coarse Moiré fringes. This effect was primarily due to the beam interference from the gratings of both layers—which have a lattice mismatch of 1.6%—when they were misoriented with respect to each other over a small angle. Nevertheless, although to a lesser extent than the monolayer, there were also Moiré fringes produced from the overlap of columnar grains. In this case, the average grain size $\langle d \rangle$ was approximately 100 nm. The SAED patterns in Fig. 4c and d correspond to the B1-NaCl structure. The diffraction rings from the multilayer were broader resulting from the superposition of reflections from TiN and (Ti,Al)N, where the latter had a slightly reduced lattice parameter. Also, the more diffuse diffraction rings of the monolayer, in contrast to the dotted rings of the multilayer, confirmed the relatively finer grain sizes and indicated a poorer crystalline perfection, i.e., the lattice distortion was retained [18].

Cross-sectional TEM images provided a more detailed picture of the microstructure and their evolution from the interface to the outer surface, as is shown in Fig. 5a and b. The monolayer had a dense fibrous structure typical of the zone T according to the zone classification proposed by Thornton [19]. This structure resulted from the ion induced defects, such as point defect clusters and small dislocation loops being trapped in the film,

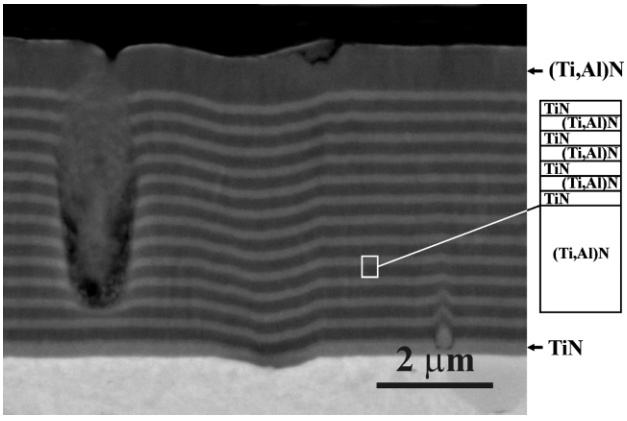

Fig. 3. Cross-sectional backscattered SEM micrograph of the multilayer showing their structure and the distortion caused by droplets and substrate surface irregularities.

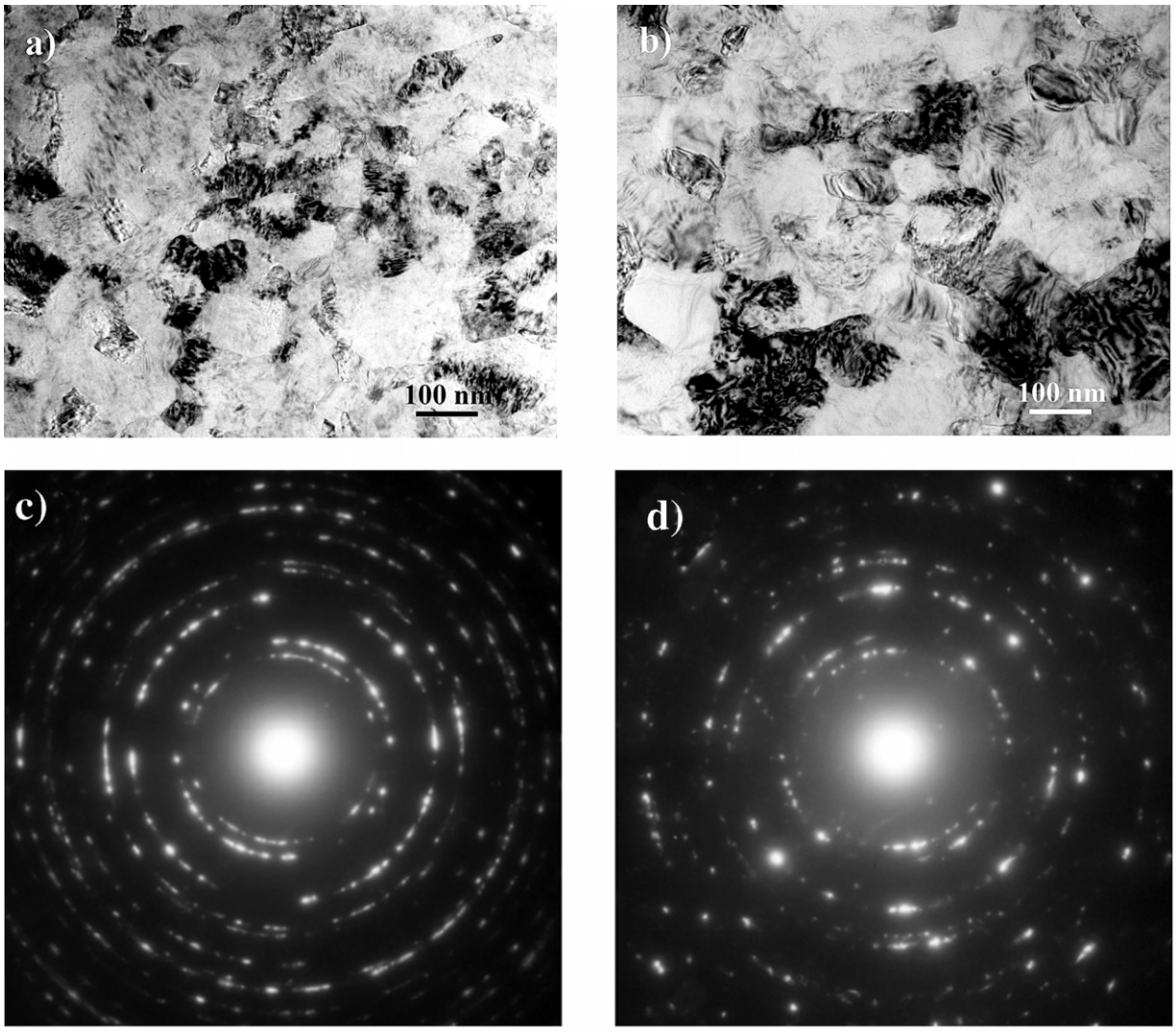

Fig. 4. Plan-view TEM images near the coating surface. (a) and (b) are bright field images of the monolayer and the multilayer, respectively. The electron diffraction patterns of the corresponding coatings are displayed in (c) and (d).

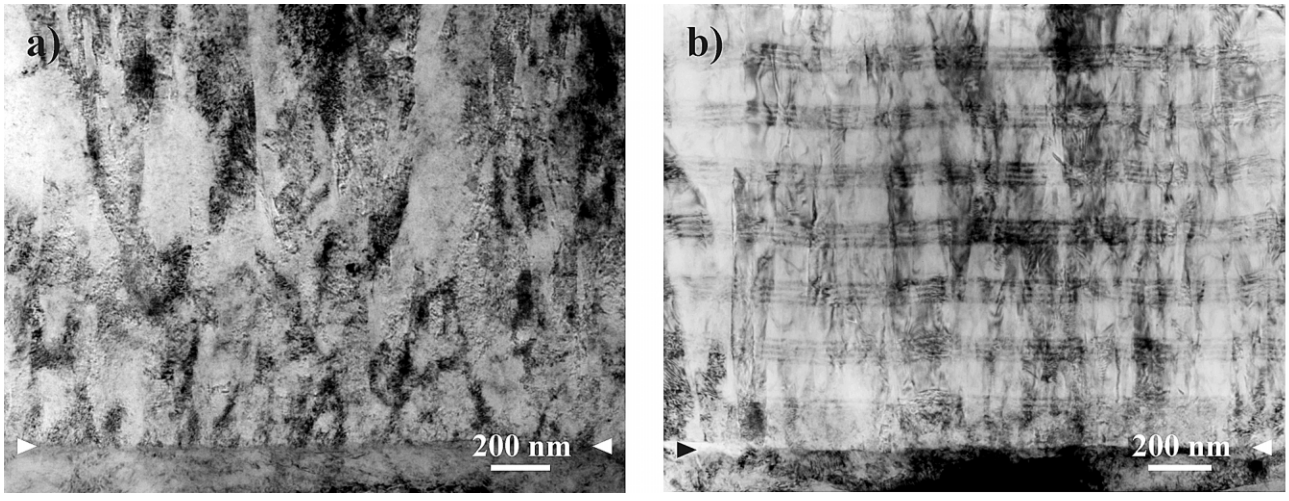

Fig. 5. Cross-sectional TEM images showing the near-interface microstructure of (a) monolayer and (b) multilayer deposited onto stainless steel substrates. The coating–substrate interface is indicated by the arrows.

and hence leading to a continuous renucleation of new grains during growth that disrupted the columnar microstructure. Thus, only a very few columns (or grains) extended through the whole coating thickness. The average column diameter was rather difficult to calculate due to their twisted nature. However, it was estimated to be approximately 50 nm. The multilayer had a more pronounced columnar microstructure, with an average column diameter increasing with film thickness from ~80 nm at the coating-substrate interface up to ~150 nm at the top of the film. This indicated a continuous competition for growth among evolving columns.

From HRTEM it was observed that the monolayer/substrate interface was formed by an amorphous interfacial region of approximately 2 nm wherein the fibre structure was nucleated. The nucleation and coalescence stages of the columnar structure faced severe competition from the others for survival. However, above this region (~140 nm) of tangled columns and, in some cases oversized grains, the fibre microstructure became more uniform. This nucleation mode is commonly observed for TiN grown on stainless steel substrate due to its lack of carbides and a large lattice mismatch between the TiN and steel substrate [20]. On the other hand, the multilayer had an abrupt interface between the TiN interlayer and the substrate. Their deposition process resulted in larger initial nuclei with a more homogeneous size, which led to the formation of wider, more uniformly sized columns that extended throughout the entire coating. The dark contrast observed on both samples below the film/substrate interface was due to strain fields. They were associated with defects within the matrix of the substrate grains induced by residual radiation-damage as a result of intense ion irradiation during ion etching.

The multilayer composition was determined by an EDS line profile using the Kα lines for the measured intensity of titanium, aluminium and nitrogen. The sensitivity factors were calculated using the theoretical cross-section method of *Zaluzec*, which was the one that gave the most reliable values. However, it should be emphasised that the concentrations presented in Fig. 6 are considered to be semi-quantitative because no standards were used for calibration. The positions where the data was taken are indicated in the TEM image. The results of the analysis showed that the layers were near-stoichiometric with respect to nitrogen (i.e. Ti:N≈1:1 and (Ti,Al):N≈1:1), and that the (Ti,Al)N layers of the superlattice had practically the same composition as the thicker layer. The undulation observed on the superlattice (cf. Fig. 5b) corresponded to the evolution of the columnar growth surfaces, which remarkably remained continuous across the grain boundaries. Their compositional modulation was measured to be $\Lambda = 21$ nm, and found to be constant throughout the film. The ratio between the TiN layer thickness and the periodicity of the superlattice was found to be regular with a value of approximately 0.46. Still, occasionally the first layer of the superlattice was thicker than expected, which can be related to instabilities in the activation of the superlattice deposition.

3.3. Formation and microstructure of macroparticles

The presence of macroparticles in the multilayer is considered as a drawback for the type of applications these coatings are designed for. Their incorporation alters significantly the surface morphology and roughness (Table 4) changing the real contact area and thus the friction and wear. Additionally, the pinholes created by their debonding have a deleterious effect on the erosion and corrosion resistance of the coatings by exposing the multilayer structure to the elements.

Fig. 7a shows a plan-view SEM micrograph of the multilayer tilted at approximately 20°. The macroparticles were uniformly distributed with an average diameter $\langle d \rangle$ ranging from tens of nanometer to a few micrometers. They were weakly bonded to the multilayer as demonstrated by the crack at the rim and by the similar morphology between the bottom of the pinhole and the coating surface. Their morphology is revealed by a fractured cross-sectional SEM micrograph containing a typical macroparticle in Fig. 7b. The macroparticles originated from the incorporation of droplets with a $\langle d \rangle \approx 1$ μm during the film growth. The height above the surrounding coating surface was similar to the droplet diameter indicating that the net deposition on top of the droplet did not differ significantly from the flat surface. For droplets with a $\langle d \rangle$ smaller than 200 nm the subsequent coating deposition covered and buried them leading to an undistorted surface. However, the columnar structure on top of the droplets was very pronounced with underdense boundaries to the bulk coating and often displaying a diameter as large as the droplet diameter. All droplets analysed were incorporated in the multilayer during the TiN growth and were never directly deposited on the steel substrate. Therefore, possible formation during the cleaning and heating stages before coating deposition, as it happens whenever cathodic-arc ion etching is used, was unlikely [21].

From SAED patterns and energy filtering transmission electron microscopy (EFTEM) it was possible to identify the phase of the droplets and hence their nature. Fig. 8a is a typical plan-view TEM image taken from a region inside of the coating showing a horizontal cross-section of a droplet. The droplet had a lower defect density compared to the bulk coating, and consisted of a core-shell structure with a few equiaxed grains and a rim with a microstructure different from the central area. Further, it was surrounded by a voided region attesting the weak bonding to the multilayer coating. The SAED patterns from the central area of the droplet were taken along different zone axis permitting the identification of the core as having the h.c.p. structure of α-Ti. As an

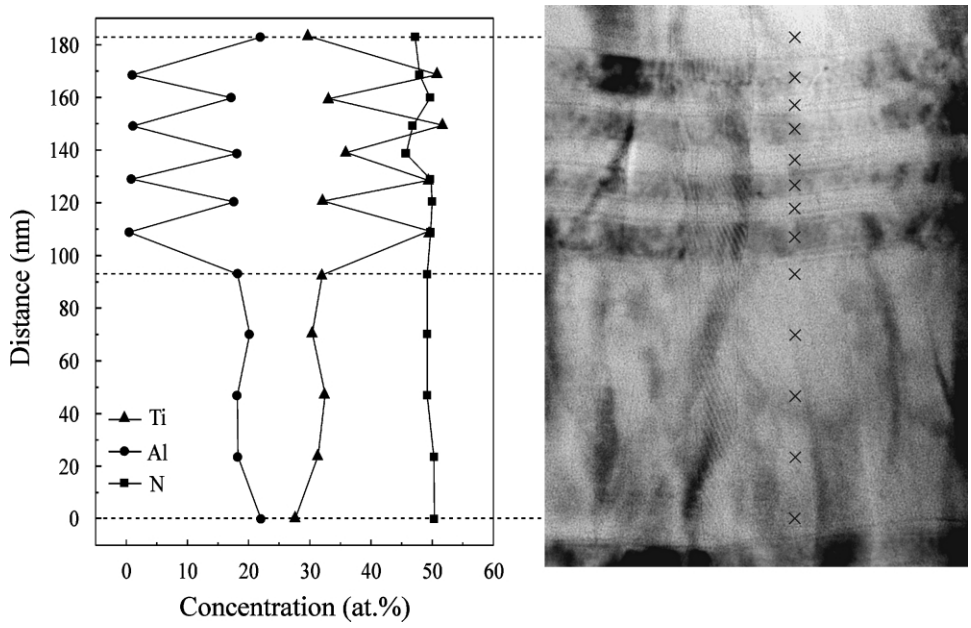

Fig. 6. EDS line profile across the (Ti,Al)N layer and the superlattice. Positions where data is taken are indicated in the TEM image. The nominal probe diameter was 1 nm and the spot acquisition time 30 s.

example, Fig. 8b shows the SAED taken along the $[0\,1\,\bar{1}\,0]$ zone axis of α-Ti. The EELS spectra of the core of the droplet displayed only the Ti L_{23}-edge located at 456 eV, giving no indication on the presence of nitrogen, whose detection limit is approximately 3 at.%. In contrast, the spectra of the rim of the droplet displayed the Ti L_{23}-edge and also the N K-edge located at 401 eV. Fig. 8c is a plan-view EFTEM image showing the droplet and the surrounding coating obtained by computing the ratio of nitrogen and titanium elemental distribution images and taking into account their partial ionisation cross-sections. The results showed that the droplet was formed by a Ti core encircled by a TiN layer, in which the nitrogen had the same intensity as in the bulk coating.

Fig. 9 shows an XTEM image of another droplet that was deposited during the growth of the TiN interfacial layer. The near spherical bottom shape and the voided boundary region formed beneath the droplet suggested that even if the droplets have left the target surface in the liquid state due to a local temperature higher than the melting point of Ti (1668 °C) [22], they had

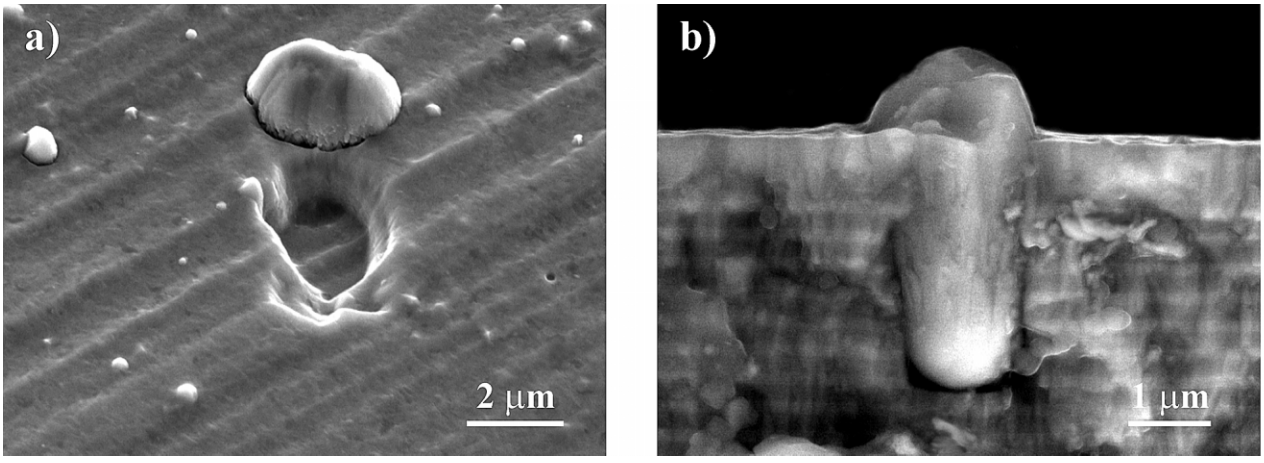

Fig. 7. SEM micrographs of the multilayer: (a) plan-view showing details from both the macroparticle and the pinhole. The sample is tilted approximately 20°; (b) fractured cross-section showing the morphology of a typical macroparticle.

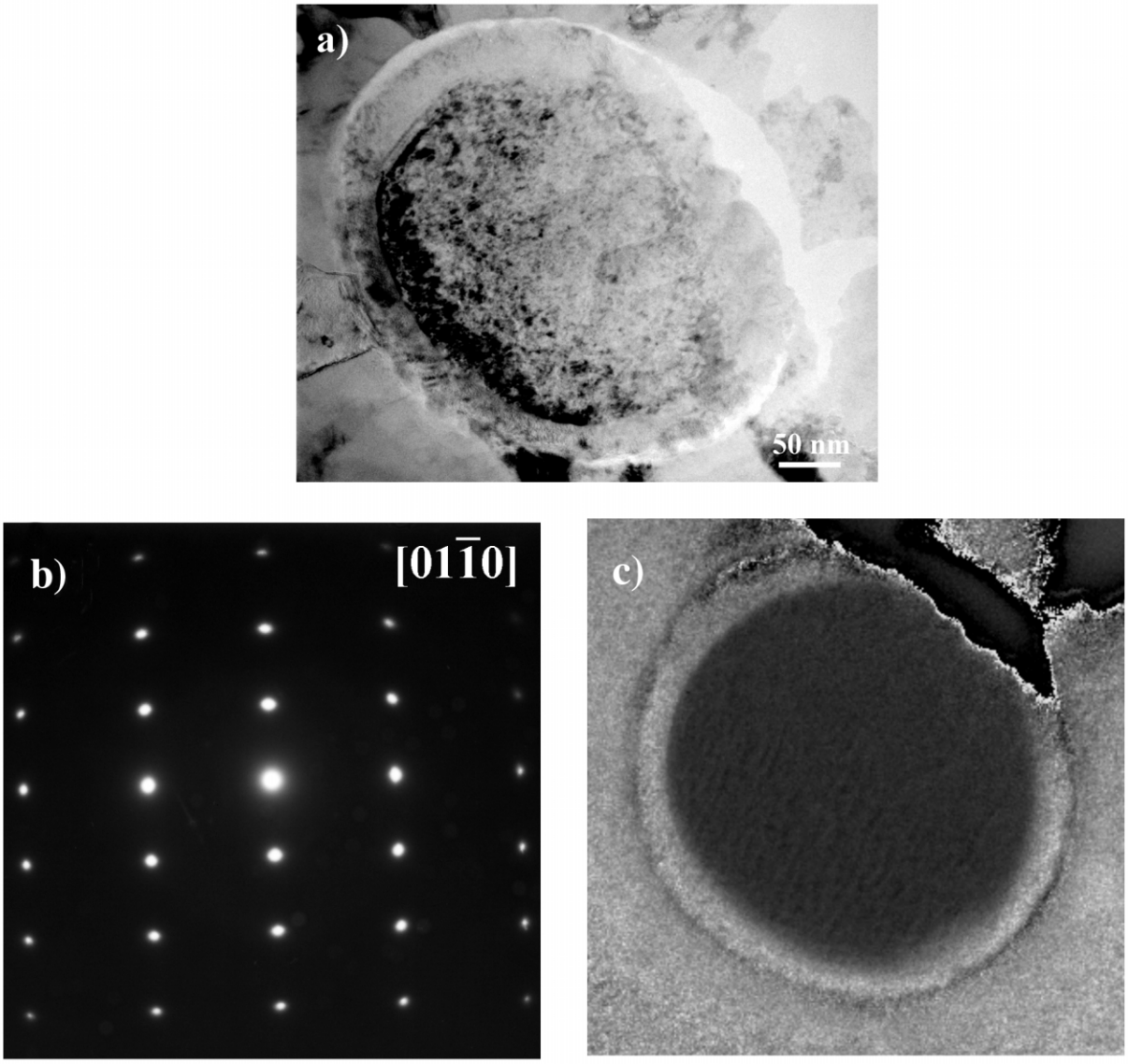

Fig. 8. Plan-view TEM image of a droplet incorporated in the multilayer: (a) bright-field image; (b) SAED pattern of the droplet core showing the diffraction spots from α-Ti phase along the [0 1 $\bar{1}$ 0] zone axis; (c) EFTEM image constructed from the ratio of nitrogen and titanium elemental maps.

solidified en route to the film surface. Cheng et al. [23] have also found numerically using thermal analysis that Ti droplets with a radius larger than 2 μm and after a flight of 200 mm from the cathode spot, remained in the liquid state. However, those with a radius smaller than 2 μm—as the ones observed here—were incorporated in the film in the solid state. The formation of the thin TiN layer on the surface of the droplets occurred upon their emission from the target and migration to the film by reacting with the ionised titanium and nitrogen particles [24]. In addition, the low density of defects observed in the first atomic layers of the nitrogen-rich rim surrounding the droplet, indicated that diffusion of N may had taken place from both the N_2 gas into the solidifying α-Ti en route to the film, and through the TiN layer at the substrate temperature (T_s) during the film growth. Ljungcrantz et al. [25] estimated the mean diffusion distance of N into the α-Ti phase, and concluded that a diffusion of 30 nm at T_s for 1 h during growth could be achieved.

The voids observed beneath the droplets were a result of the shadowing effect of the incoming atomic flux in combination with the limited adatom mobility. This reduced adhesion of the droplets combined with the developing compressive stresses of the multilayer when cooling from the deposition temperature, triggered the

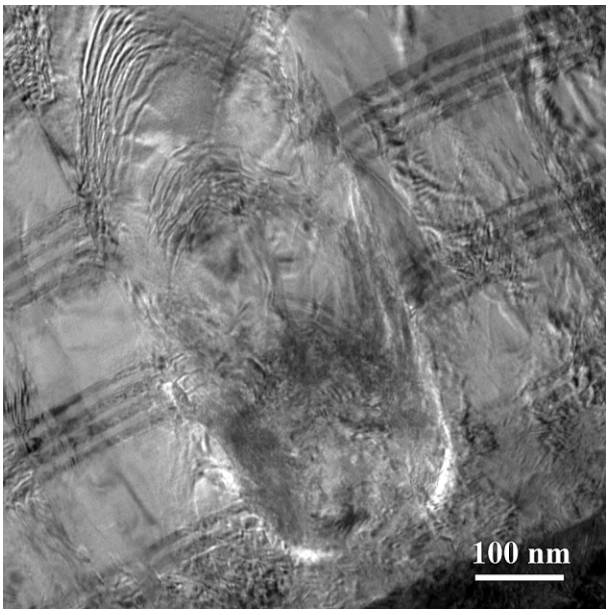

Fig. 9. Cross-sectional TEM image of a macroparticle incorporated during deposition of the TiN interfacial layer. The voided boundary region beneath the droplet has a brighter contrast. See also the multilayer distortion on top of the droplet.

removal of the ones close to the surface. As a consequence the presence of pinholes on the surface of the multilayer coating was not surprising.

4. Conclusions

The commercially available monolayer TiN and multilayer TiN/(Ti,Al)N coatings were studied concerning their crystal structure, stress state, and microstructural features. The TiN exhibited a polycrystalline structure, was highly (1 1 1) textured, and was in a state of compressive stresses in the order of 4–5 GPa. The coating had a dense fibrous structure with an average column diameter estimated to be ~50 nm. The multilayer consisted of (Ti,Al)N layers and a superlattice of TiN and (Ti,Al)N with a periodicity of 200 nm. The compositional modulation within the superlattice itself was 21 nm. The multilayer had also a polycrystalline structure and was slightly (3 1 1) textured, having each component a different compressive stresses, being 3–4 GPa for the (Ti,Al)N layer and 8–10 GPa for the TiN layer. The magnitude of the compressive stresses was found to have a dependency on the layer thickness, and type of substrate material. When compared to the monolayer, the multilayer had a more pronounced columnar microstructure with the average column diameter increasing with film thickness (from 80 up to 150 nm) hinting a continuous competition for growth among the evolving columns.

The microstructure and composition of micrometer-sized droplets found in the multilayer were examined. It was demonstrated that they were incorporated in the solid state during deposition of the TiN material, and that they were weakly bonded to the bulk coating. The droplets were formed by a core structure with few equiaxed grains having the α-Ti phase and a rim of a thin TiN layer exhibiting a gradient in defect density. This could be explained as the effect of nitrogen diffusion into the core of the droplet during both the *route* to the film and at the growing film surface. Voided regions were always observed beneath the droplets as a consequence of shadowing of the atomic flux. Their reduced adhesion prompted the removal of the ones close to the surface leaving craters behind with exposed multilayer.

Acknowledgments

The work described in this paper has been funded by the TNO Institute of Industrial Technology and the Netherlands Institute for Metals Research. The deposition of the PVD coatings on steel substrates by Balzers Group is acknowledged.

References

[1] R. Buhl, H.K. Pulker, E. Moll, Thin Solid Films 80 (1981) 265.
[2] D.S. Rickerby, P.J. Burnett, Surf. Coat. Technol. 33 (1987) 191.
[3] J. Desmaison, P. Lefort, M. Billy, Oxidation Metals 13 (1979) 5.
[4] U. Wahlström, L. Hultman, J.-E. Sundgren, F. Adibi, I. Petrov, J.E. Greene, Thin Solid Films 235 (1993) 62.
[5] K.S. Chan, M.Y. He, J.W. Hutchinsson, J. Mater. Sci. Eng. A 167 (1993) 57.
[6] M.Y. He, A.G. Evens, Int. J. Solids Structure 31 (1994) 3443.
[7] E. Bergmann, U.S. Patent No. 4877505, 31 October 1989.
[8] J.A. Thornton, J. Vac. Sci. Technol. A 4 (1986) 3059.
[9] N.J.M. Carvalho, Ph.D. Thesis, University of Groningen, The Netherlands, 2001.
[10] D.R. McKenzie, Y. Yin, W.D. McFall, N.H. Hoang, J. Phys. Cond. Mater. 8 (1996) 5883.
[11] W.D. Sproul, J. Vac. Sci. Technol. A 12 (1994) 1595.
[12] E. Zoestbergen, N.J.M. Carvalho, J.Th.M. De Hosson, Surf. Eng. 17 (2001) 1.
[13] J.A. Sue, Surf. Coat. Technol. 54/55 (1992) 154.
[14] H. Oettel, R. Wiedemann, Surf. Coat. Technol. 76/77 (1995) 265.
[15] J.-D. Kamminga, Th.H. De Keijser, R. Delhez, E.J. Mittemeijer, Thin Solid Films 317 (1998) 169.
[16] H. Randhawa, J. Vac. Sci. Technol. A 4 (1986) 2755.
[17] B.E. Jacobson, R.F. Bunshah, R. Nimmagadda, Thin Solid Films 54 (1978) 107.
[18] D.T. Quinto, J. Vac. Sci. Technol. A 6 (1988) 2149.
[19] J.A. Thornton, Annu. Rev. Mater. Sci. 7 (1977) 239.
[20] M.K. Hibbs, B.O. Johansson, J.-E. Sundgren, U. Helmersson, Thin Solid Films 122 (1984) 115.

[21] I. Petrov, P. Losbichler, D. Bergstrom, J.E. Greene, W.-D. Münz, T. Hurkmans, T. Trinh, Thin Solid Films 302 (1997) 172.
[22] R.L. Boxman, S. Goldsmith, Surf. Coat. Technol. 48 (1991) 51.
[23] Z. Cheng, M. Wang, J. Zou, Surf. Coat. Technol. 92 (1997) 50.
[24] M.-H. Shiao, F.-S. Shieu, Thin Solid Films 386 (2001) 27.
[25] H. Ljungcrantz, L. Hultman, J.-E. Sundgren, G. Håkansson, L. Karlsson, Surf. Coat. Technol. 63 (1994) 123.